Journal of the Earth & Space Physics. Vol. 32, No. 3, 2006, P. 11-21

Least square minimization for depth and shape determination through Micro-gravity data

Ardestani, E. V*.

*Institute of Geophysics, University of Tehran, P.O. Box 14155- 6466, Tehran, Iran and Center of Excellence in Geomatics Engineering and Disaster Management, Survey Engineering Department, University of Tehran

(Received: 2 Jan 2006 , Accepted: 19 Sep 2006)

Abstract

The least-square minimization approaches for determination of depth, shape and amplitude coefficient expressed by Abdolrahman et al. (2001) for sphere and horizontal cylinder is used for rectangular prisms as synthetic models with and without random noises. The method is also applied for real sources producing micro-gravity data .The capability of the method is tested and discussed in this paper.

Key words: Least-square minimization, Depth, Shape factor, Amplitude coefficient, Rectangular prism, Micro-gravity data

1 INTRODUCTION

Simple geometrically models such as spheres and cylinders have usually been considered in gravity interpretation.

In most cases the shape of the model is assumed and the depth variable may be obtained through different methods such as least-square minimization (Abdolrahman et al., 1991).

Determination of the shape by least-square minimization is also expressed by Abdolrahman et al. (1995), Abdolrahman and El-Arabi, (1993) and Abdolrahman et al. (2001).

The method used in the last paper will be tested against rectangular prisms and real sources.

2 LEAST-SQUARE MINIMIZATION

The gravity anomaly expression for a horizontal cylinder is given by Nettelton, (1976),

$$g(X_i, Z, q) = \frac{kZ}{(X_i^2 + Z^2)^q} \qquad (1)$$

Where $k = 2\pi G\rho R^2$, q is the shape factor and is 1 for a horizontal cylinder (Abdolrahman et al., 1989), G is the gravitational constant, ρ is the contrast density and R is the radius of the cylinder.

Clearly $g(X_i, Z, q)$ attains its maximum at X=0. The maximum value is where m is equal to 1 for horizontal cylinder.

$$g(max) = \frac{k}{Z^{2q-m}} \qquad (2)$$

where m is equal to 1 for the horizontal cylinder.

Using equation (2), equation (1) can be written in a normalized form as,

$$\frac{g(X_i, Z, q)}{g(max)} = \frac{Z^{2q}}{(X_i^2 + Z^2)^q} \qquad (3)$$

Taking the logarithm of the both sides of equation (3) we obtain

$$F(X_i, Z, q) = \ln\left[\frac{g(X_i, Z, q)}{g(max)}\right] = q \ln\frac{Z^2}{(X_i^2 + Z^2)} \qquad (4)$$

Equation (4) gives the following value at $X_i = A$,

$$F(A) = q \ln\frac{Z^2}{(A^2 + Z^2)} \qquad A = \pm 1,2,3,... \qquad (5)$$

Substituting equation (5) in equation (4), we obtain the following nonlinear equation in the depth (Z) we have,

$$F(X_i, Z) = F(A) * W(X_i, Z) \qquad (6)$$

Where,

$$W(X_i, Z) = \frac{\ln\frac{Z^2}{X_i^z + Z^2}}{\ln\frac{Z^2}{A^2 + Z^2}} \qquad (7)$$

The unknown depth (Z) in equation (6) can be determined by minimizing the squared differences between observed and calculated anomalies, (Abdolrahman et al., 2001),

$$\varphi(Z) = \sum_{i=1}^{N} \left[L(X_i) - F(A) * W(X_i, Z) \right]^2 \qquad (8)$$

Where $L(X_i)$ is the logarithm of the normalized $\left(g(X_i, Z, q)/g(\max)\right)$ observed gravity anomaly at X_i.

Setting the derivative of $\varphi(Z)$ to zero with respect to Z yields,

$$f(Z) = \sum_{i=1}^{N} \left[L(X_i) - F(A) * W(X_i, Z) \right] W^*(X_i, Z) = 0 \qquad (9)$$

Where

$$W^*(X_i, Z) = \frac{d}{dZ}(W(X_i, Z)). \qquad (10)$$

Equation (9) can be solved for Z using numerical methods.

Substituting the computed depth Z_c as a fixed parameter in equation (5), we obtain

$$F(X_i, q) = q \ln \frac{Z_c^2}{(A^2 + Z_c^2)} \qquad (11)$$

Again applying the least-squares method the unknown q (shape factor) can be obtained from The following equation (Abdolrahman et al. 2001),

$$q_c = \frac{\sum_{i=1}^{N} L(X_i) \ln \frac{Z_c^2}{X_i^2 + Z_c^2}}{\sum_{i=1}^{N} \ln \frac{Z_c^2}{X_i^2 + Z_c^2}}. \qquad (12)$$

Substituting the computed depth (Z_c) and shape factor (q_c) in equation (1) as fixed parameters we have,

$$D(x_i) = \frac{k z_c}{(X_i^2 + Z_c^2)^{q_c}} \qquad (13)$$

Where $D(X_i)$ is the observed gravity data. Finally applying the least-squares method to equation. (13) yields, (Abdolrahman et al., 2001),

$$k_c = \frac{\sum_{i=1}^{N} \frac{D(X_i)}{(X_i^2 + Z_c^2)^{q_c}}}{\sum_{i=1}^{N} \frac{Z_c}{(X_i^2 + Z_c^2)^{q_c}}} \qquad (14)$$

Then Abdolrahman et al. (2001) proposed measuring the correctness of the fit between the observed and the computed gravity data for each A value.

3 PROCEDURES

Applying the above method a computer code in MATLAB is prepared.

Approximating the section of a horizontal cylinder as a rectangular prism on a profile along the cylinder the effects of the cylinders are computed by Talwani's (1959) method and then are contaminated by different amounts of random noises through NORMRND commend (MATLAB commend for generating random numbers from normal distribution) and considered as observed anomalies.

Five points of profile around the maximum value (peak of the anomalies) are selected.

The equation (2) is then minimized for Z value by FMINUNC (MATLAB commend which finds the minimum of a function of several variables) considering an initial value for depth (z_0) and q=1.

Having z_c, q_c and k_c the computed gravity anomalies are obtained through equation (7).

The squared differences between the observed and computed values (Sum) are calculated and the results are plotted.

4 RECTANGULAR PRISMS

We used the method expressed in the previous section for rectangular prisms considering the similarity of the shapes in two dimensional cases with horizontal cylinders.

The first model is demonstrated in Figure (1b).

The computed gravity effects are obtained through equation (6) for different sets of observed gravity anomalies (figure 1a). The results for different A and Z_0 are shown in table 1.

The second model is shown in figure 2b and the observed and computed gravity effects in figure 2a.

The results are reflected in table 2. In this deeper model the depths belong to the top of the rectangular prism as the former depths (table 1) show the center of the prism.

In both models of figures 1 and 2 the computed depths do not depend on the initial guesses of depths.

The models in figures 3b, 4b are the same as figures. 1b and 2b but with the noise

(10 percent) added to the observed gravity values.

The results of these models are demonstrated in tables 3 and 4.

Two complex models are considered in figurs. 5b and 6b for testing the capability of the method and the results are demonstrated in tables 5 and 6 respectively.

Table 1. Depths and shape factor for model 1.

Z_0 (m)	A	z_c (m)	q_c	k_c (μGal.m)	Sum (μGal)
10	1	19.56	0.994	1618.04	1992.29
20	1	19.56	0.994	1618.04	1992.29
5	1	19.56	0.994	1684.04	1992.29
5	2	19.56	0.994	1618.04	1992.29

Table 2. Depths and shape factor for model 2.

Z_0 (m)	A	z_c (m)	q_c	k_c (μGal.m)	Sum (μGal)
15	1	23.2	0.996	1284.38	633.29
25	1	23.2	0.996	1288.49	633.312
10	1	23.2	0.996	1286.82	633.292
20	2	23.2	0.996	1286.82	633.292

Table 3. Depths and shape factor for model 3.

Z_0 (m)	A	z_c (m)	q_c	k_c (μGal.m)	Sum (μGal)
5	1	22.58	1.003	2011.812	1584.981
10	1	22.578	1.003	2011.653	1584.977
20	1	22.578	1.003	2011.807	1584.981
20	2	22.578	1.003	2011.807	1584.981

Table 4. Depths and shape factor for model 4.

Z_0 (m)	A	z_c (m)	q_c	k_c (μGal.m)	Sum (μGal)
5	1	33.64	1.00	1732.39	207.89
5	1	33.64	1.00	1732.39	207.89
10	1	33.595	0.997	1732.46	207.85
20	3	33.64	1.00	1697.17	207.89

Table 5. Depths and shape factor for model 5.

Z_0 (m)	A	z_c (m)	q_c	k_c (μGal.m)	Sum (μGal)
5	1	25.415	1.0022	3410.436	2859.368
10	1	25.419	1.0024	3410.22	2859.462
20	1	25.415	1.002	3410.396	2859.367
20	2	25.415	1.0022	3410.396	2859.367

Table 6. Depths and shape factor for model 6.

Z_0 (m)	A	z_c (m)	q_c	k_c (μGal.m)	Sum (μGal)
5	1	24.755	1.001	2375.948	1547.038
10	1	24.753	1.001	2374.019	1547.011
20	1	24.754	1.001	2375.22	1547.028
20	2	24.754	1.001	2375.22	1547.028

In all models the sum-squared differences between the observed and computed values (Sum) are quite big but still the computed depths (z_c) and shape factors (q_c) are acceptable.

It is clear that the results are quite independent of the initial guess (at least up to four times the least guess and for shallow depths) for depth (Z_0) and A which is a great capability of the model and proves the excellent ability of the computer program.

5 FIELD EXAMPLES

A micro-gravity survey detecting the cavities and sink-holes has been carried out in the power plant close to Hamedan (Iran).

One of the anomalies detected is chosen (figure 7) and a Bouguer gravity profile (AB) is considered.

To have an initial guess for initial depth and also testing the results the Euler depths of the anomaly computed through GEOSOFT is also demonstrated in figure 8.

The results for different initial depth and A are as follows,

The observed and computed gravity are reflected in figure 9.

As the method is actually described for a simple shape such as a cylinder, there is a relatively big difference between the observed and computed curves but at the same time the computed Z seems to be quite reasonable.

The second profile is shown in the Bouguer anomaly map of another cavity in the same power plant (figure 10). The Euler depths are demonstrated in figure 11.

The method is used and the results for different Z_0 and A are reflected in table 8.

The depths in both anomalies are quite appropriate and approved by other methods and drilling.

Again although there is a difference between observed and calculated curves in figure 6 at least the computed depth is quite reasonable.

6 CONCLUSION

The method is quite effective particularly for depth and for shape factor determination in spite of the probable big sum squared difference in real examples.

The independency of the results to the initial guess of depth is a great advantage of the method.

ACKNOWLEDGEMENT

The author is thankful to the Institute of Geophysics for all its supports.

Table 7

Z_0 (m)	A	z_c (m)	q_c	k_c (μGal.m)	Sum (μGal)
5	1	4.83	1.01	3279.867	1516.078
10	1	4.83	1.018	3279.137	1516.02
10	2	4.83	1.018	3279.137	1516.03

Table 8

Z_0 (m)	A	z_c (m)	q_c	k_c (μGal.m)	Sum (μGal)
5	1	23.093	0.988	2828.413	1102.82
15	1	23.139	0.992	2900.322	1102.86
15	0.5	23.139	0.992	2900.322	1102.862

REFERENCES

Abdolrahman, E. M., and Sharafeldin, S. M., 1995a, A least-squares minimization approach to shape determination from gravity data. Geophysics, **60**, 589-590.

Abdolrahman, E. M., El-Araby, H. M., El-Araby, T. M., and Abo-Ezz E. R., 2001, Three least-squares minimization coefficient determination from gravity data. Geophysics, **66**, 1105-1109.

Abdolrahman, E. M., and El-Arabi, T. M., 1993, A least-square minimization approach to depth determination from moving average residual gravity anomalies. Geophysics, **59**, 1779-1784.

Abdolrahman, E. M., Bayoumi, A. I., and El-Arabi, H. M., 1991, A least-square minimization approach to invert gravity data. Geophysics, **56**, 11-118.

Abdolrahman, E. M., Bayoumi, A. I., Abdelhady, Y. E., Gobashy, M. M., and El-Arabi, H. M., 1989, Gravity interpretation using correlation factors between successive least-square residual anomalies, Geophysics, **54**, 1614-1621.

Nettelton, L. L., 1942, Gravity and magnetic calculations. Geophysics, **7**, 293-310.

Talwani, M., Worzel, J. L., Landisman, M., 1959, Rapid computation for two-dimensional bodies with application to the Mendocino Submarine Fracture zone. Geophys. Res, **64**, 49-59.

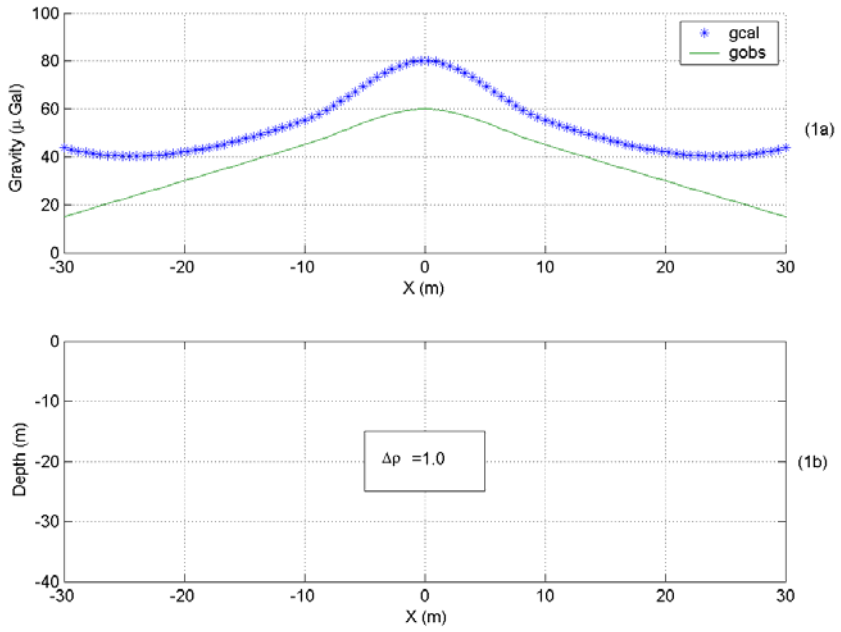

Figure 1. (a) Observed and computed gravity anomalies (μGal). (b) Rectangular prism.

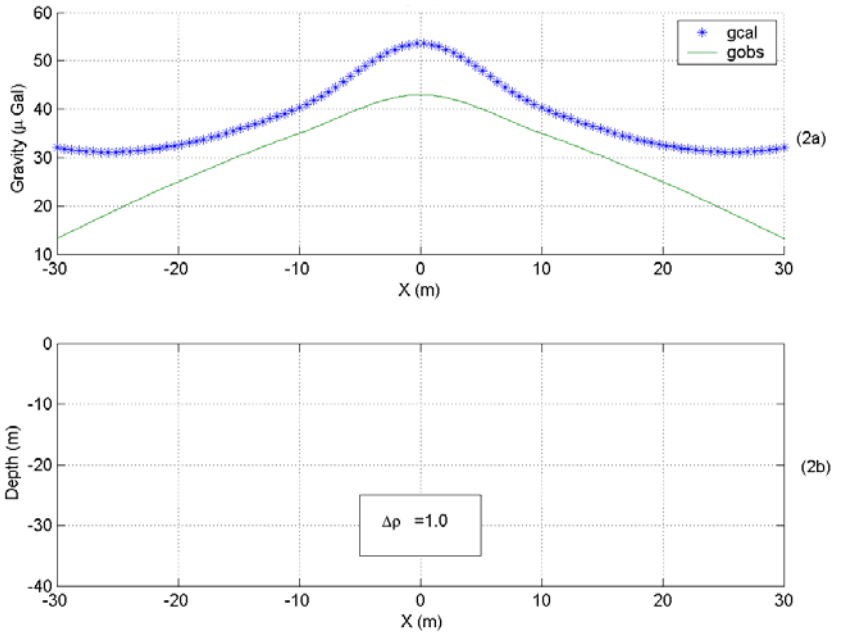

Figure 2. (a) Observed and computed gravity anomalies (μGal). (b) Rectangular prism.

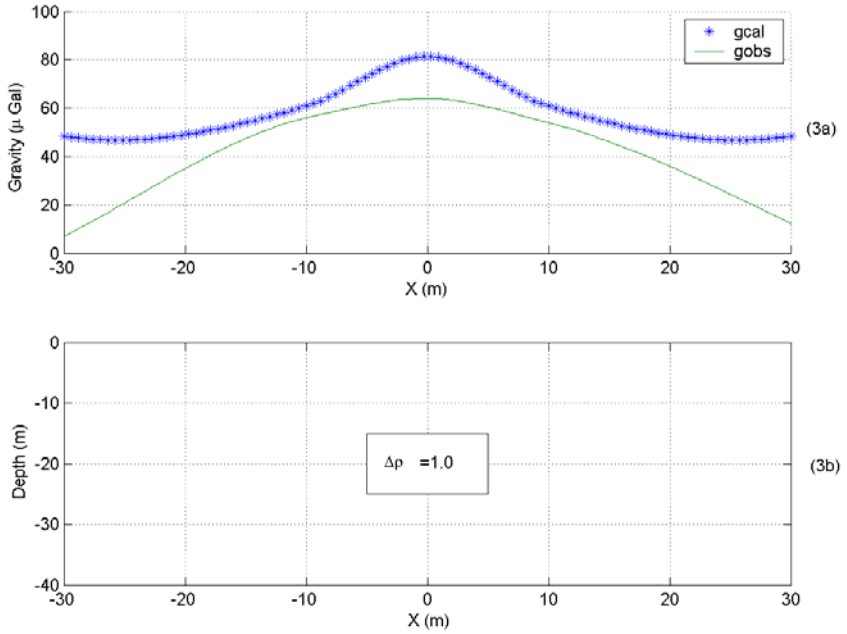

Figure 3. (a) Observed and computed gravity anomalies (μGal). (b) Rectangular prism.

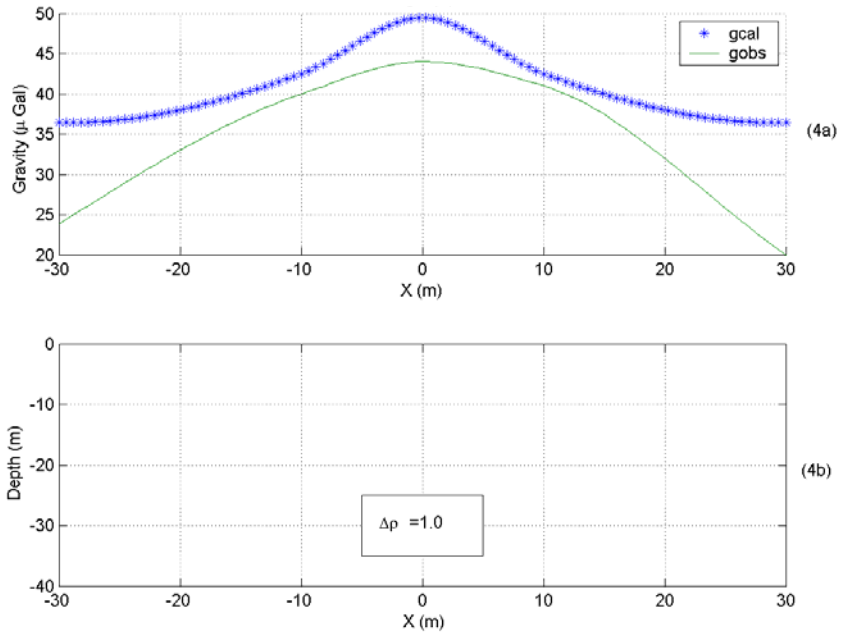

Figure 4. (a) Observed and computed gravity anomalies (μGal). (b) Rectangular prism.

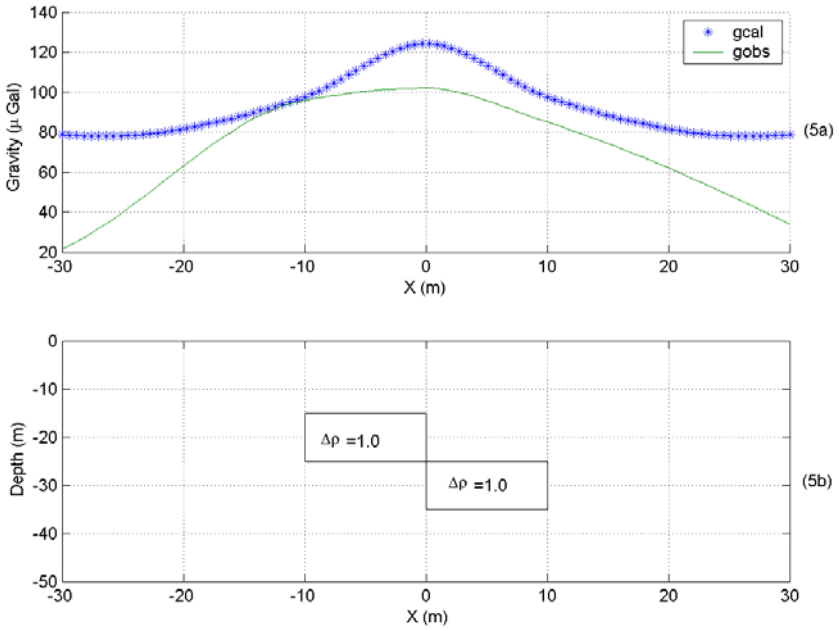

Figure 5. (a) Observed and computed gravity anomalies (μGal). (b) Rectangular prism.

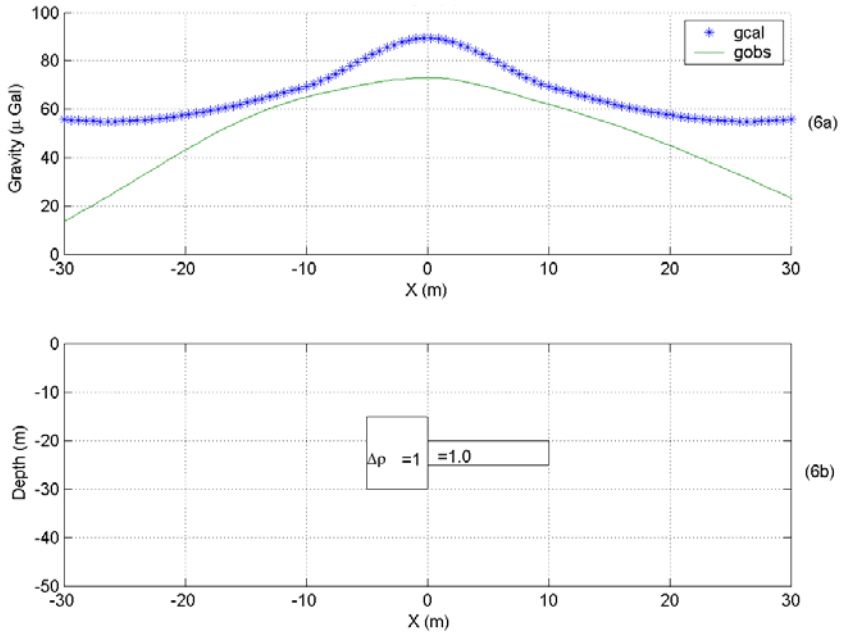

Figure 6. (a) Observed and computed gravity anomalies (μGal). (b) Rectangular prism.

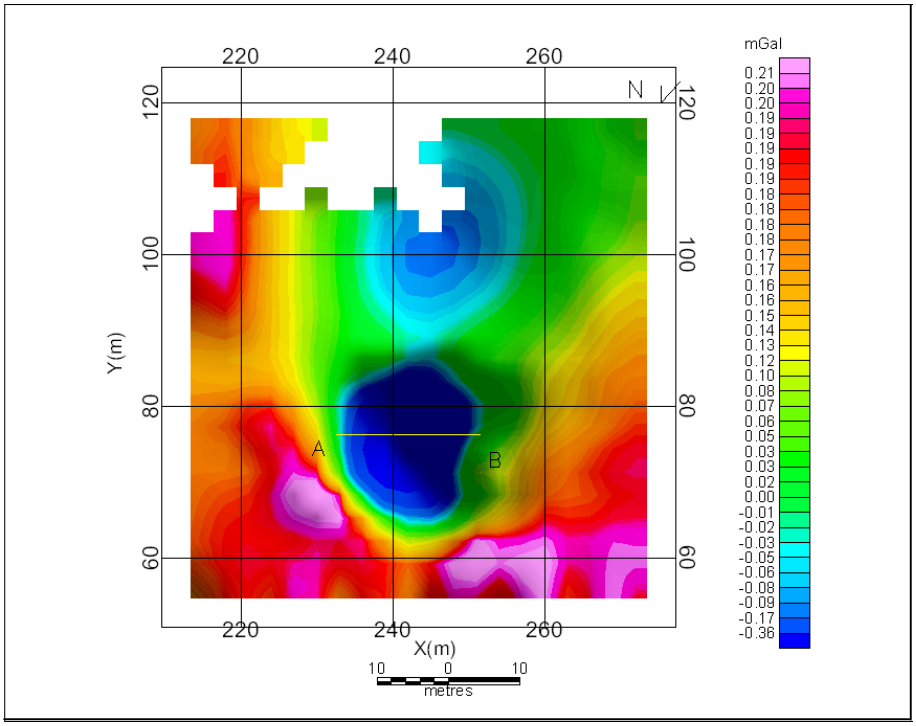

Figure 7. Bouguer anomalies (mGal).

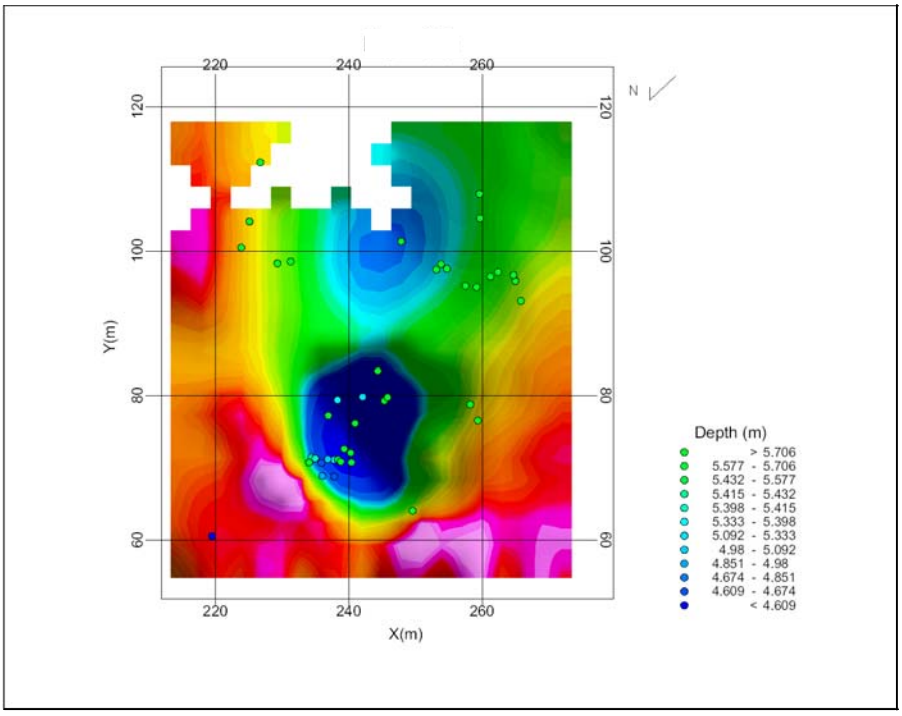

Figure 8. Euler depths (m).

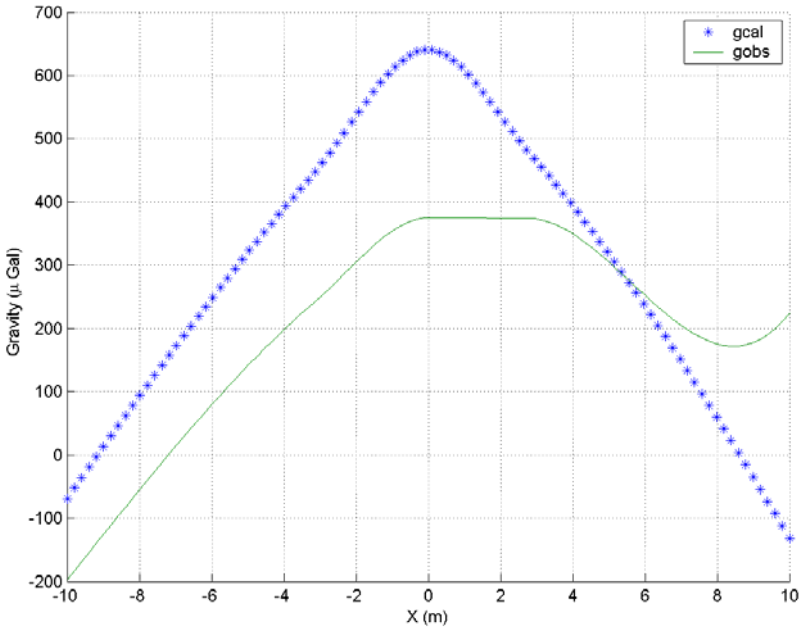

Figure 9. Observed and computed gravity anomalies (mGal).

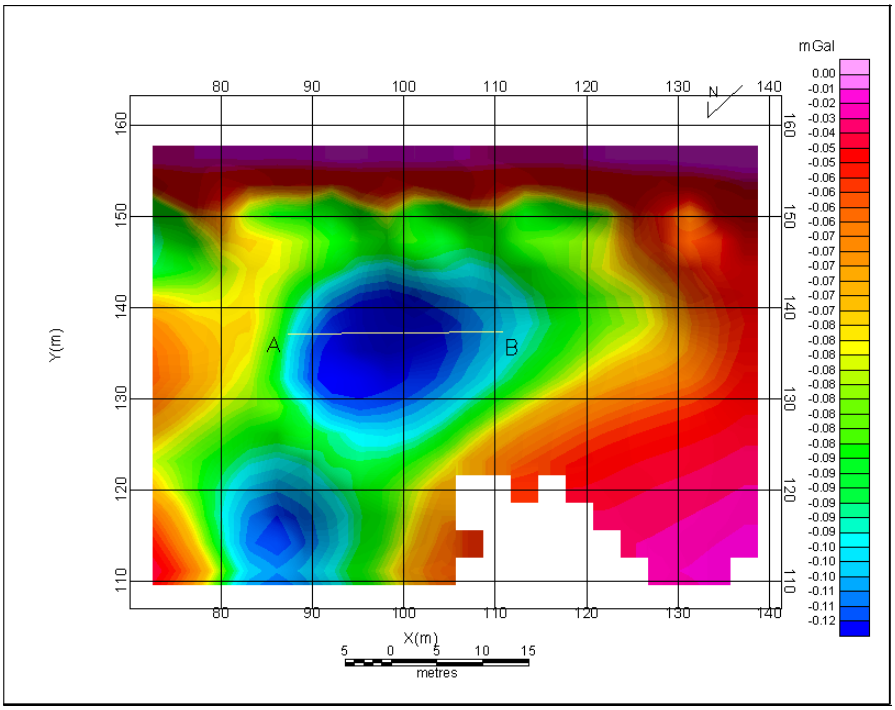

Figure 10. Bouguer anomalies (mGal).

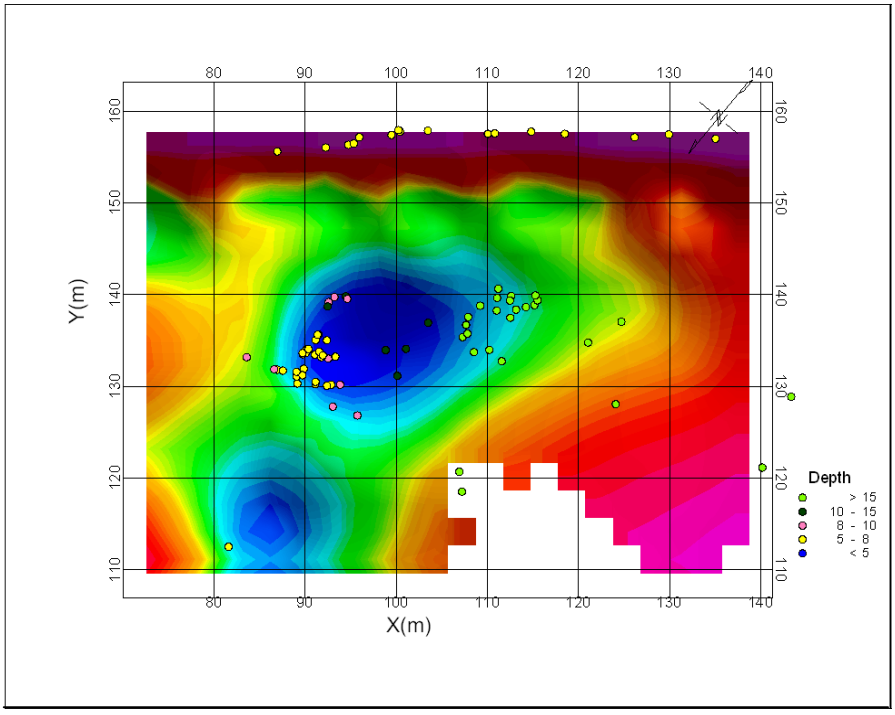

Figure 11. Euler depths (m).

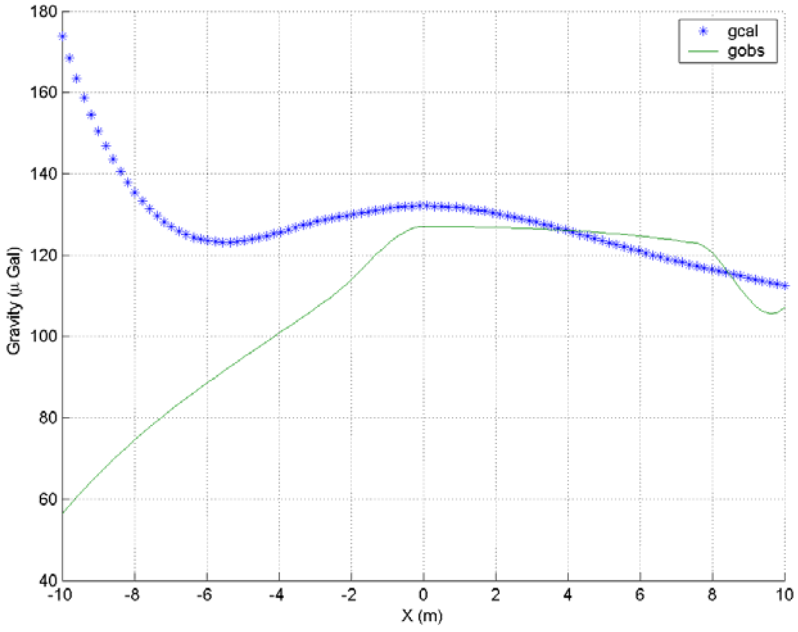

Figure 12. Observed and computed gravity anomalies (mGal).